A&A 572, A56 (2014)
DOI: 10.1051/0004-6361/201424534

Astronomy & Astrophysics

ASTE observations in the 345 GHz window towards the HII region N113 of the Large Magellanic Cloud

S. Paron[1,2], M. E. Ortega[1], M. Cunningham[3], P. A. Jones[3], M. Rubio[4], C. Fariña[5], and S. Komugi[6]

[1] Instituto de Astronomía y Física del Espacio (IAFE, CONICET-UBA), CC 67, Suc. 28, 1428 Buenos Aires, Argentina
e-mail: sparon@iafe.uba.ar
[2] FADU and CBC, Universidad de Buenos Aires, Argentina
[3] School of Physics, University of New South Wales, Sydney, NSW 2052, Australia
[4] Departamento de Astronomía, Universidad de Chile, Casilla 36-D, Santiago, Chile
[5] Isaac Newton Group of Telescopes, 38700, La Palma, Spain
[6] National Astronomical Observatory of Japan, 2-21-1 Osawa, Mitaka, Tokyo 181-8588, Japan

Received 4 July 2014 / Accepted 9 September 2014

ABSTRACT

Aims. The HII region N113 is located in the central part of the Large Magellanic Cloud (LMC) with an associated molecular cloud that is very rich in molecular species. Most of the previously observed molecular lines cover the frequency range 85–270 GHz. Thus, a survey and study of lines at the 345 GHz window is required for a more complete understanding of the chemistry and excitation conditions of this region.
Methods. We mapped a region of 2.′5 × 2.′5 centred at N113 using the Atacama Submillimeter Telescope Experiment in the ^{13}CO $J = 3-2$ line with an angular and spectral resolution of 22″ and 0.11 km s^{-1}. In addition, we observed 16 molecular lines as single pointings towards its centre.
Results. From the ^{13}CO $J = 3-2$ map we estimate the local thermodynamic equilibrium (LTE) and virial masses in about 1×10^4 and 4.5×10^4 $M_\odot$ for the molecular cloud associated with N113. From the dust continuum emission at 500 μm we additionally obtain a mass of gas of 7×10^3 $M_\odot$. Towards the cloud centre we detected emission from ^{12}CO, ^{13}CO, C^{18}O (3–2), HCN, HNC, HCO$^+$, C_2H (4–3), and CS (7–6); these are the first reported detections of the HCN, HNC, and C_2H (4–3) lines from this region. We confirm the detection of CS (7–6), which was previously tentatively detected. From analysing the HCN, HNC, and C_2H lines we suggest that they might be emitted from a photodissociation region (PDR). Moreover, we suggest that the chemistry involving the C_2H lines in N113 is probably similar to that in Galactic PDRs. We analysed the HCN $J = 4-3$, $J = 3-2$, and $J = 1-0$ lines with the code RADEX and we conclude that we observe very high density gas, between some 10^5 and 10^7 cm^{-3}.

Key words. galaxies: ISM – Magellanic Clouds – HII regions – ISM: individual objects: N113 – ISM: molecules

1. Introduction

The HII region N113 is located in the central part of the Large Magellanic Cloud (LMC). It hosts two H_2O masers, of which one is the most intense maser of the Magellanic Clouds (Whiteoak & Gardner 1986; Lazendic et al. 2002; Imai et al. 2013), and an OH maser (Brooks & Whiteoak 1997). This region is associated with a clumpy molecular cloud (Seale et al. 2012) that is active in star formation. Three young stellar clusters, NGC 1874, NGC 1876, and NGC 1877, are related to N113 (Bica et al. 1992) and several young stellar objects (YSOs) have been found embedded in the molecular gas associated with this HII region (Gruendl & Chu 2009; Seale et al. 2009; Sewiło et al. 2010; Seale et al. 2012; Carlson et al. 2012).

One of the main motivations of molecular observational studies towards different regions in the LMC (e.g. Johansson et al. 1994) is to study a low-metallicity interstellar medium (ISM), whose physical conditions may resemble those that existed in the early Milky Way and that therefore can shed light on the primeval processes of star formation. The molecular cloud associated with N113 is one of the richest in the LMC and has been studied often, presenting observations with different resolutions and sensitivities of many molecular lines (Wong et al. 2006; Wang et al. 2009, and references therein). However, most of the molecular lines observed towards N113 cover the frequency range 85−270 GHz (see Chin et al. 1997; Wang et al. 2009). Only three lines were successfully observed at higher frequencies: ^{13}CO and ^{12}CO $J = 3-2$ at 330.56 and 345.79 GHz, respectively, and HCO$^+$ $J = 4-3$ at 356.73 GHz. Thus, a survey and study of molecular lines at the 345 GHz window (324−372 GHz) is required for a more complete understanding of the chemistry and excitation conditions of the region. To do this, we used the Atacama Submillimeter Telescope Experiment (ASTE) to map N113 in the ^{13}CO $J = 3-2$ transition and to observe 16 molecular lines within the 345 GHz window towards its centre.

2. Observations and data reduction

The molecular observations were performed between July and August 2010 with the 10 m ASTE telescope (Ezawa et al. 2004). We used the CATS345 GHz band receiver, a two single-band SIS receiver, which is remotely tunable in the LO frequency range of 324−372 GHz. The XF digital spectrometer was set to a bandwidth and spectral resolution of 128 MHz and 125 kHz. The spectral velocity resolution was 0.11 km s^{-1} and the half-power beamwidth (HPBW) was 22″ at 345 GHz. The system temperature varied from $T_{sys} = 150$ to 250 K and the main beam efficiency was $\eta_{mb} \sim 0.65$.

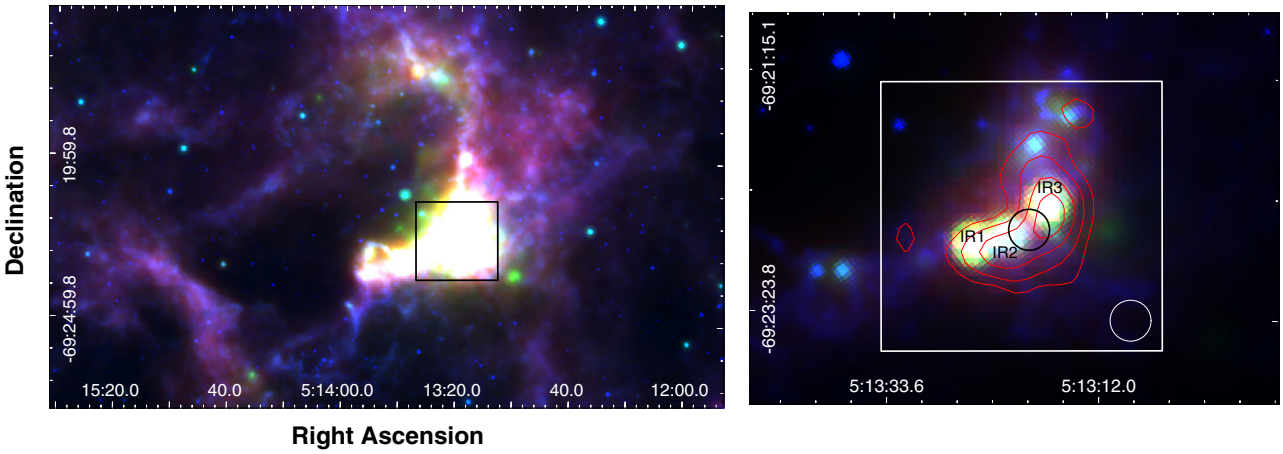

Fig. 1. *Left*: three-colour image where the 8, 24, and 70 μm emission obtained from the IRAC and MIPS cameras of the *Spitzer* Space Telescope (from SAGE *Spitzer*; Meixner et al. 2006) are presented in blue, green, and red, respectively. The black box shows the region mapped in the ^{13}CO $J = 3-2$ line with an angular resolution of 22″. *Right*: zoom-in of the mapped region (white box). The colour code is the same as in the *left image*, but the scales are different. The red contours correspond to the ^{13}CO $J = 3-2$ emission integrated between 230 and 245 km s^{-1} with levels of 2.5, 4.0, 6.0, and 8.0 K km s^{-1}. The FWHM beam size of the observations is included in the bottom right corner of the region. The black circle corresponds to the position where the 16 molecular lines were observed as single pointings.

Table 1. Observed molecular lines towards N113.

Molecular line	Integ. time (s)	Detection
^{12}CO (3–2)	200	yes
^{13}CO (3–2)	1160	yes
C^{18}O (3–2)	1160	yes
H_2D^+ (1, 0–1, 1)	1520	no
H_2CO (5–4)	1520	no
c-C_3H_2 (9–8)	1440	no
H_3O^+ (3, 2–2, 2)	480	no
HCN (4–3)	1520	yes
HNC (4–3)	800	yes
CS (7–6)	600	yes
HCO^+ (4–3)	600	yes
CH_3CN (18–17)	1280	no
CH_3CN (19–18)	1620	no(?)*
C_2H (4–3)	1620	yes
HNCO (15–14)	1280	no
DCO^+ (5–4)	1520	no

Notes. (*) See Sect. 3.2.

The data were reduced with NEWSTAR[1] and the spectra processed using the XSpec software package[2]. The spectra were Hanning-smoothed to improve the signal-to-noise ratio, and in some cases a boxcar smoothing was as applied as well. Polynomials between first and third order were used for baseline fitting.

Several molecular lines in the 345 GHz window were observed towards the centre of N113 at RA = 05^{h}13^{m}19.5^s, Dec = −69° 22′ 37.9″, J2000 as single pointings (black circle in Fig. 1-right). In Table 1 we list the observed molecular lines and integration times; they indicate whether the detection was positive or not. Additionally, we mapped a 2.′5 × 2.′5 region centred on RA = 05^{h}13^{m}20^s, Dec = −69°22′35.5″, J2000 in the ^{13}CO $J = 3-2$ line (white square in Fig. 1-right). This observation was performed in on-the-fly mapping mode and achieved an angular sampling of 6″.

3. Results and discussion

3.1. Molecular cloud

Figure 1 (left) is a three-colour image of the mid/far-IR emission in the N113 area where the mapped region in the ^{13}CO $J = 3-2$ line is indicated with a black square. Figure 1 (right) shows a zoom-in of the mapped region with a different colour scale, which allows identifying some point-like sources in the IR emission. The ^{13}CO $J = 3-2$ emission integrated between 230 and 245 km s^{-1} is presented in contours and shows that the curved and elongated morphology of the molecular cloud agrees well with the IR emission. The surveyed area is populated by 18 O and early-B stars (both on the main sequence and evolved), most of them with spectral types derived via UBV photometric data (Wilcots 1994). A few have spectroscopic observations as a mid-OV star (target s1 in the Wilcots study), sources BI 104 and BI 105 observed by Massey et al. (1995) that are B0.5V and O7V stars, and the more widely studied supergiant star, HD269217, which is of type B2[e] (e.g. Kastner et al. 2010). The main concentration of high-mass YSOs (Seale et al. 2012) and intermediate-mass YSO candidates (Carlson et al. 2012) are located in projection along the CO emission, a configuration commonly found in massive star-forming regions (e.g. Povich et al. 2009; Book et al. 2009; Chen et al. 2010). The three conspicuous IR sources observed in Fig. 1 (right) that appear over the molecular concentration, marked as IR1, IR2, and IR3, are coincident with the compact radio continuum sources detected by Brooks & Whiteoak (1997) and with three YSOs (from south-east to north-west: 051325.09-692245.1, 051321.43-692241.5, and 051317.69-692225.0) catalogued by Seale et al. (2012) and Carlson et al. (2012). As discussed in Wong et al. (2006), these sources might be young ionizing stars that affect the molecular gas and probably contribute to the birth of new stars.

The morphology and velocity distribution of the molecular gas related to N113 is shown in Fig. 2, where the ^{13}CO $J = 3-2$ emission is presented in a series of channel maps in the range of 231−242 km s^{-1}, integrated in steps of 1 km s^{-1}.

[1] Reduction software based on AIPS developed at NRAO, extended to treat single-dish data with a graphical user interface (GUI).

[2] XSpec is a spectral line reduction package for astronomy that has been developed by Per Bergman at Onsala Space Observatory.

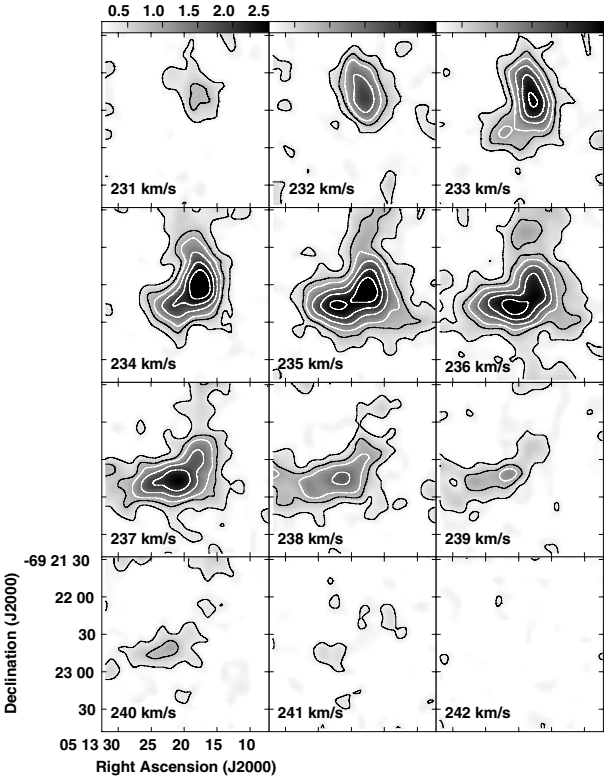

Fig. 2. Integrated velocity channel maps of the ^{13}CO $J = 3{-}2$ emission every 1 km s^{-1}. The greyscale is displayed at the top of the first panel and is in K km s^{-1}, the contour levels are 0.3, 0.7, 1, 2, and 2.5 K km s^{-1}.

The curved and elongated molecular cloud is resolved into two clumps, one located towards the north-west and peaking at 233 km s^{-1}, the other one slightly eastwards of the centre of the surveyed region, peaking at 236 km s^{-1}.

To roughly estimate the molecular mass, we assumed local thermodynamic equilibrium (LTE). We calculated the excitation temperature from

$$T_{\rm ex}(3 \rightarrow 2) = \frac{16.59 \text{ K}}{\ln[1 + 16.59 \text{ K}/(T_{\rm max}(^{12}\text{CO}) + 0.036 \text{ K})]}, \quad (1)$$

where $T_{\rm max}(^{12}\text{CO})$ is the ^{12}CO peak temperature towards the centre of the region, obtaining $T_{\rm ex} \sim 20$ K. We derived the ^{12}CO and ^{13}CO optical depths, τ_{12} and τ_{13}, using (e.g. Scoville et al. 1986)

$$\frac{^{12}\text{T}_{\rm mb}}{^{13}\text{T}_{\rm mb}} = \frac{1 - \exp(-\tau_{12})}{1 - \exp(-\tau_{12}/X)}, \quad (2)$$

where $^{12}T_{\rm mb}$ and $^{13}T_{\rm mb}$ are the peak temperatures of the ^{12}CO and ^{13}CO $J = 3{-}2$ lines at the centre of the region, and $X = 50$ is the assumed isotope abundance ratio (Wang et al. 2009). The result is $\tau_{12} \sim 9.5$ and $\tau_{13} \sim 0.2$, which indicates that the ^{13}CO $J = 3{-}2$ line is optically thin. Thus, we estimated its column density from

$$N = 8.28 \times 10^{13}\, e^{\frac{15.87}{T_{\rm ex}}} \frac{T_{\rm ex} + 0.88}{1 - e^{\frac{-15.87}{T_{\rm ex}}}} \frac{1}{J(T_{\rm ex}) - J(T_{\rm BG})} \int T_{\rm mb}\, {\rm d}v \quad (3)$$

with

$$J(T) = \frac{h\nu/k}{\exp(\frac{h\nu}{kT}) - 1}. \quad (4)$$

To obtain the molecular hydrogen column density $N(\text{H}_2)$ we assumed an abundance ratio of $[\text{H}_2/^{13}\text{CO}] = 1.8 \times 10^6$, estimated by Garay et al. (2002) towards the giant molecular complex No. 37 in the LMC. Almost the same value has been obtained for N159W (Heikkilä et al. 1999), which like N113 is associated with a prominent star-forming region. Finally, the mass was derived from

$$M = \mu\, m_{\rm H} \sum_i \left[D^2\, \Omega_i\, N_i(\text{H}_2)\right], \quad (5)$$

where Ω is the solid angle subtended by the beam size, D is the distance (50 kpc), $m_{\rm H}$ is the hydrogen mass, and μ is the mean molecular weight, assumed to be 2.8 by taking into account a relative helium abundance of 25%. We summed over all beam positions of the molecular structure displayed in contours in Fig. 1 (right panel). The obtained mass is about 1×10^4 $M_\odot$, which is somewhat lower than the 8.2×10^4 $M_\odot$ estimated by Wong et al. (2006) from the ^{12}CO $J = 1{-}0$ line using a standard Galactic CO to H_2 conversion factor ($N_{\rm H_2}/I_{\rm CO} = 2.0 \times 10^{20}$ cm^{-2} (K km s^{-1})$^{-1}$). This discrepancy probably arises because the ^{13}CO $J = 3{-}2$ and the ^{12}CO $J = 1{-}0$ map different extensions of the molecular cloud; alternatively the Galactic CO to H_2 conversion factor used by Wong et al. might not be appropriate for N113.

From the average of the ^{13}CO $J = 3{-}2$ emission towards the molecular structure we obtain an averaged spectrum with $\Delta v = 5.3$ km s^{-1}. We roughly approximated the molecular cloud with a spherical shape of radius 35″ ($R = 8.8$ pc) and considered a density profile of $\rho \propto r^{-1}$. From this we estimated the virial mass according to MacLaren et al. (1988),

$$\frac{M_{\rm vir}}{M_\odot} = 190 \left(\frac{R}{\rm pc}\right) \left(\frac{\Delta v}{\rm km\ s^{-1}}\right)^2, \quad (6)$$

which gives $\sim 4.5 \times 10^4$ $M_\odot$.

Additionally, we estimated the mass of gas of the N113 cloud from the continuum emission at the far-infrared regime arising from the dust. To do so we obtained the integrated flux of the continuum emission at 500 μm using the calibrated level 2 PLW SPIRE image extracted from the Herschel Data Archive (ObsID:1342202224). Figure 3 displays the 500 μm emission with contours of the ^{13}CO $J = 3{-}2$, showing that both emissions are very similar in morphology and size. From the radiative transfer equation and assuming an optically thin medium we

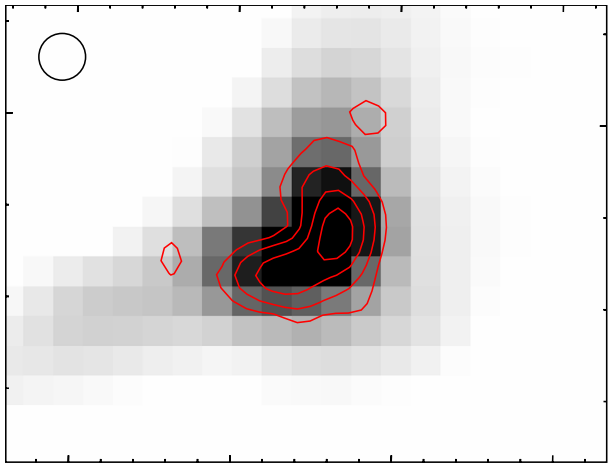

Fig. 3. 500 μm emission obtained from SPIRE in the Herschel Space Observatory (from Herschel HERITAGE; Meixner et al. 2010, 2013) with the same ^{13}CO $J = 3{-}2$ contours as shown in Fig. 1 (right). The FWHM beam size of the molecular observations is included in the top left corner. The angular resolution of the SPIRE image is about 36″.

Table 2. Line parameters for the molecular lines presented in Figs. 4 and 5.

Molecular line	$\int T_{\rm mb} dv$ (K km s^{-1})	$T_{\rm mb}$ peak (K)	$v_{\rm LSR}$ (km s^{-1})	Δv (*FWHM*) (km s^{-1})
^{12}CO (3–2)	66.20 ± 2.20	9.90 ± 0.30	235.84 ± 0.10	6.25 ± 0.20
^{13}CO (3–2)	9.52 ± 1.50	1.73 ± 0.32	236.58 ± 0.47	5.23 ± 1.10
C^{18}O (3–2)	0.35 ± 0.10	0.05 ± 0.02	235.68 ± 0.55	4.73 ± 1.70
CS (7–6)	0.54 ± 0.18	0.08 ± 0.02	235.15 ± 0.80	5.75 ± 1.20
HCO$^+$ (4–3)	3.40 ± 0.20	0.47 ± 0.10	233.90 ± 0.95	7.15 ± 1.50
HCN (4–3)	0.70 ± 0.15	0.09 ± 0.02	234.28 ± 0.75	8.22 ± 1.50
HNC (4–3)	0.35 ± 0.10	0.08 ± 0.02	234.87 ± 0.70	3.85 ± 1.00

estimated the gas mass in the cloud as

$$M_{\rm gas} = \frac{S_\lambda D^2}{\kappa_{\rm d}(\lambda) x_{\rm d} B_\lambda(T_{\rm d})}, \quad (7)$$

where S_λ, D, $\kappa_{\rm d}(\lambda)$, $x_{\rm d}$, and $B_\lambda(T_{\rm d})$ are the integrated flux at 500 μm, the distance, the dust absorption coefficient, the dust-to-gas mass ratio, and the Planck law at the $T_{\rm d}$ dust temperature, respectively. We considered the obtained integrated flux at 500 μm to be of about 50 Jy, a distance of 50 kpc, $\kappa_{\rm d}(500\,\mu{\rm m}) = 1.14$ for the LMC (Weingartner & Draine 2001), a $T_{\rm d}$ of about 24 K, and $x_{\rm d} = 1.7 \times 10^{-3}$ (Verdugo et al. 2011) and derived a gas mass of about 7×10^3 $M_\odot$. This value is almost two orders of magnitude lower than the mass estimated by Wang et al. (2009) from the 1.2 mm dust continuum. The $M_{\rm vir}/M_{\rm gas}$ ratio is higher than unity, as found in several clouds in N11 (Herrera et al. 2013), a bright HII region in the LMC hosting several star clusters.

3.2. Molecular lines

In Figs. 4 and 5 we present the spectra of the molecular lines that were successfully observed towards the position indicated with a black circle in Fig. 1 (right). Figure 4 shows the CO isotopologues and Fig. 5 the emission of the detected rarer lines. The line parameters given in Table 2 were obtained from single-component Gaussian fits. All the spectra have signals well above the 3σ, except for the C^{18}O J = 3–2 line, for which the signal is evident but the noise is high. The HNC and HCN lines are detected for the first time towards N113 in the J = 4–3 transition. On the other side, the CS J = 7–6 line was tentatively detected by Wang et al. (2009), and we confirm its detection here. Our CS central velocity and Δv agree, within the errors, with the previous tentative detection. Taking into account that the critical density of the HCN J = 4–3 line is about 10^8 cm^{-3} (Takakuwa et al. 2007), we conclude that we observe a high-density molecular clump, which agrees with the conspicuity of the CS J = 7–6 line, which also is a tracer of high-density gas.

Figure 6 shows the obtained spectrum in the frequency range 349.30–349.43 GHz, which is populated by several lines and fine-structure components of C_2H and CH_3CN. The frequencies at which molecular emission lines are expected according to the NIST data base[3] are indicated in the figure and listed in Table 3. In the spectrum presented in Fig. 6 two peaks can be distinguished that are most likely due to the C_2H (4–3) fine-structure transitions. The peak centred on 349.342 GHz is composed of two C_2H blended hyperfine lines and probably of one line of the CH_3CN 19–18 transition. The other peak, centred on 349.403 GHz, is also composed of two C_2H blended hyperfine lines. Chin et al. (1997) and Wang et al. (2009) have reported the

[3] http://www.nist.gov/pml/data/micro/index.cfm

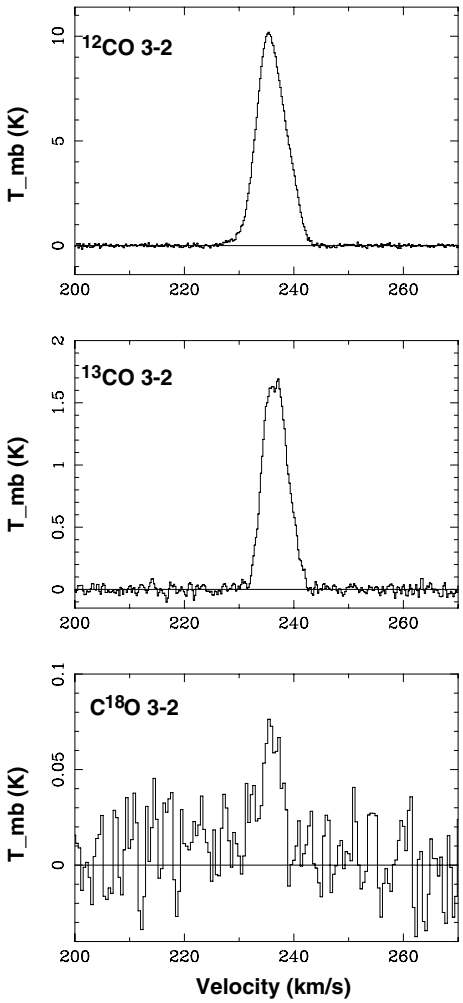

Fig. 4. CO isotopologues obtained towards the centre of N113. The rms noise levels of each spectrum are 80, 35, and 30 mK, respectively, and the channel spacings are about 0.2 km s^{-1} for ^{12}CO and ^{13}CO, and 0.4 km s^{-1} for C^{18}O.

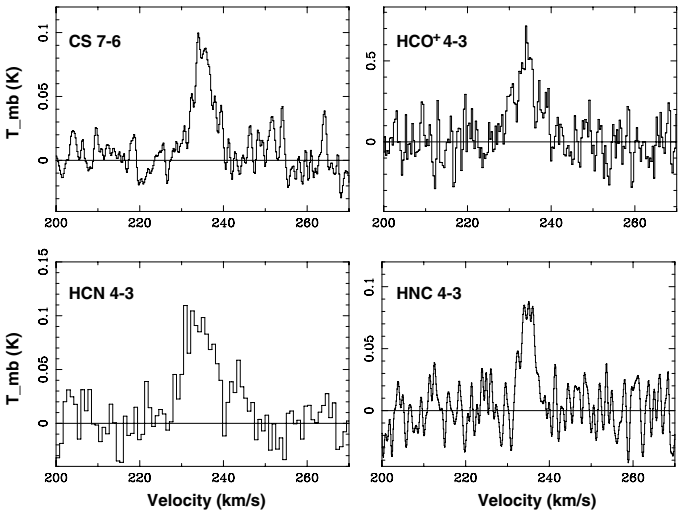

Fig. 5. Spectra of CS J = 7–6 and HCO$^+$, HCN, and HNC J = 4–3 obtained towards the centre of N113. The rms noise levels of each spectrum are 14, 90, 20, and 13 mK, respectively, and the channel spacings are about 0.2 km s^{-1} for CS, HCO$^+$, and HNC, and 1.2 km s^{-1} for HCN.

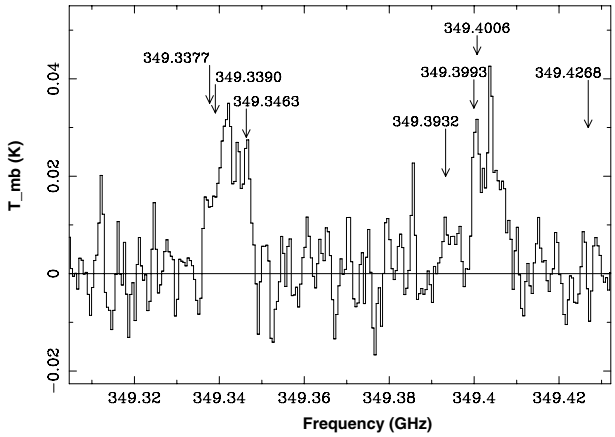

Fig. 6. Spectrum in the frequency range 349.30−349.43 GHz. The arrows indicate the frequencies at which molecular emission lines are expected according to the NIST data base (see Table 3). The rms noise is about 6 mK and the channel spacing is about 0.5 MHz.

Table 3. Molecular lines within the 349.30−349.43 GHz range.

Frequency (GHz)	Molecule	Transition (quantum numbers)
349.3377	C_2H	4–3 J = 9/2−7/2 F = 5−4
349.3390	C_2H	4–3 J = 9/2−7/2 F = 4−3
349.3463	CH_3CN	19(4)–18(4)
349.3932	CH_3CN	19(3)–18(3)
349.3993	C_2H	4–3 J = 7/2−5/2 F = 4−3
349.4006	C_2H	4–3 J = 7/2−5/2 F = 3−2
349.4268	CH_3CN	19(2)–18(2)

Notes. See spectrum in Fig. 6.

detection of C_2H (1−0) J = 3/2−1/2 F = 2−1 and 1−0 lines towards N113, and here we present the first detection of C_2H (4−3) towards this region. It is not possible to confirm the detection of the CH_3CN 19(4)−18(4) line, which is probably blended in the peak centred on 349.345 GHz. In addition the non-detection of the CH_3CN 18−17 line, a lower transition, also suggests a non-detection for the J = 19−18 transition.

Beuther et al. (2008) observed C_2H (4–3) towards a Galactic sample of star-forming regions in different evolutionary stages, including infrared dust clouds (IRDCs), high-mass protostellar objects (HMPOs), and ultracompact HII regions (UCHIIs). They found that the C_2H lines are detected independently of the evolutionary stage of the sources, but the UCHIIs regions exhibit line widths in both C_2H (4−3) main peaks that are significantly broader than the others objects (on average about 5.5 km s^{-1}). Assuming that the peaks in the spectrum of Fig. 6 are due exclusively to emission of C_2H, and converting the frequency into velocity, we measured the FWHM of the two peaks to be 6.8 and 6.4 km s^{-1}, which indicates that both are broad lines like those measured by Beuther et al. (2008) towards UCHIIs. This result agrees with the presence of the compact radio continuum sources detected by Brooks & Whiteoak (1997) in N113. Furthermore, the position at which the molecular lines were observed in this study lies between the two most intense continuum sources in the study of Wong et al. (2006) (sources 2 and 3; IR2 and IR3 in Fig. 1-right). The authors have estimated that the equivalent of one or two O6 stars is needed to produce the measured fluxes in the radio continuum (at 24 and 86 GHz) towards source 2, which, as discussed in their study, are probably

Table 4. Integrated intensity ratios towards N113.

Ratio	This work	Chin et al. (1997) (all J = 1−0)	Wang et al. (2009)
$\frac{^{12}CO}{^{13}CO}$	6.9 ± 1.1	7.28 ± 0.70	4.50 ± 0.16 (J = 3–2)
$\frac{^{13}CO}{C^{18}O}$	27.0 ± 8.8*	35.8 ± 3.1	39.8 ± 2.7 (J = 1–0)
$\frac{HCO^+}{HCN}$	4.8 ± 1.1	1.34 ± 0.06	1.47 ± 0.10 (J = 1–0) 2.15 ± 0.47 (J = 3–2)
$\frac{HCN}{HNC}$	2.0 ± 0.7	2.8 ± 0.2	2.6 ± 0.2 (J = 1–0)
$\frac{HNC}{HCO^+}$	0.10 ± 0.03	0.26 ± 0.01	0.26 ± 0.01 (J = 1–0)

Notes. (*) Tentative ratio because of the high noise in the $C^{18}O$ spectrum.

young ionizing stars that affect the molecular gas. The C_2H can be formed and/or replenished after destruction in earlier stages in PDRs through $C_2H_2 + h\nu \rightarrow C_2H + H$. The neutral-neutral reaction $CH_2 + C \rightarrow C_2H + H$ can also produce C_2H, where the precursor carbon atom is formed through the photodissociation of CO (Miettinen 2014, and references therein). Therefore, we suggest that the chemistry involving this radical in N113 is similar to the chemistry in Galactic PDRs.

The observed integrated intensity ratios are listed in Table 4 for the lines presented in Table 2, together with a comparison with ratios obtained using the J = 1−0 transitions from Chin et al. (1997) and Wang et al. (2009) for the transitions indicated in the table. Our results agree with the ratios obtained from lower transitions, except for the ratios of HCO^+/HCN and HNC/HCO^+. The HCO^+/HCN ratio is higher than unity, as was found in several Magellanic giant molecular clouds, suggesting that the ion abundance is higher than in Galactic clouds, where this ratio was found to be lower than unity (Stacey et al. 1991; Chin et al. 1997). This must be due to higher UV fields in the Magellanic environments. Additionally, the low nitrogen abundance in the LMC (e.g. Hunter et al. 2007; Bekki & Tsujimoto 2010) can also contribute to the increment of the HCO^+/HCN ratio. Furthermore, it seems that the HCO^+/HCN ratio increases for increasing rotational transitions, which suggests that the physical conditions in N113 may favour the excitation of the HCO^+ higher transitions more efficiently than those of HCN. If the HCO^+ and HCN emission occur in the same region, the increment in the HCO^+/HCN ratio with the rotational transitions may reflect different critical densities, with HCN being selectively de-excited at higher transitions. Even though the E_u/k_B factor is similar in both molecular species, their critical densities vary between different J_u−J_l transitions (n_{crit}(HCN)/n_{crit}(HCO^+) ∼5−7 for J = 1−0, 3–2, and 4–3; Papadopoulos 2007). Similar cases of this HCO^+/HCN ratio behaviour were found towards the Galactic NGC 1333-IRAS 2A outflow (Jørgensen et al. 2004) and towards the nuclear region of M82 (Seaquist & Frayer 2000). The HCN/HNC ratio is higher than unity in the J = 4−3 line, as is the case for the lower transitions, which supports the prediction by Chin et al. (1997) that the ratio would be high in warm gas that is subject to strong UV heating, but approaches unity in cloud cores. Wang et al. (2009) also pointed out that HCN/HNC ratio higher than unity may indicate a PDR scenario, which agrees with the C_2H chemistry discussed above.

Using the derived HCN J = 4−3 parameters listed in Table 2 and the HCN J = 3−2 and J = 1−0 parameters presented in Wang et al. (2009), we performed a non-LTE study of this

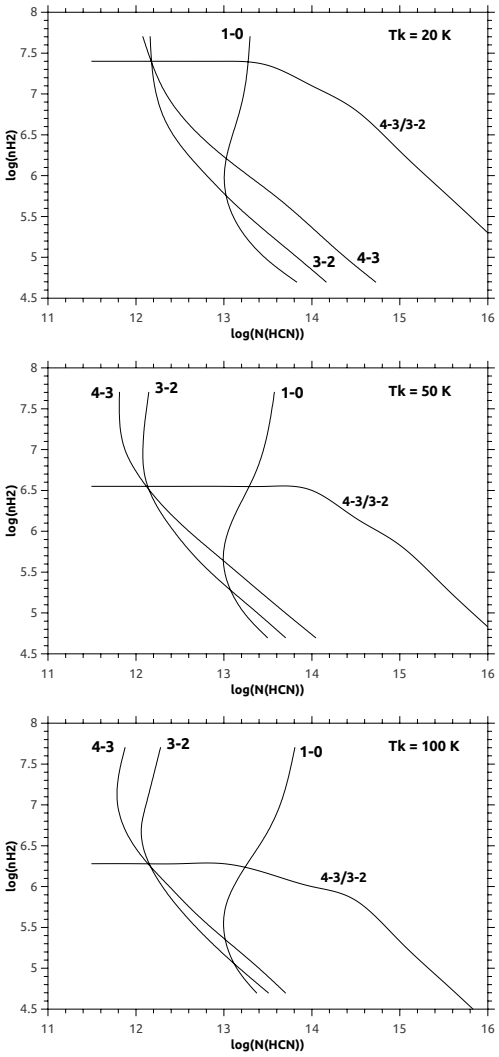

Fig. 7. Radex calculations for the HCN $J = 4–3$ and 3–2 lines for kinetic temperatures of 20, 50, and 100 K. The results for HCN $J = 1–0$ are included for comparison with Wang et al. (2009).

molecular species using the code RADEX (van der Tak et al. 2007). This code uses the mean escape probability approximation for the radiative transfer equation. As in Wang et al. (2009), we corrected for beam dilution by calculating $T'_{\rm mb} = T_{\rm mb}/\eta_{\rm bf}$, with $\eta_{\rm bf} = \theta_{\rm s}^2/(\theta_{\rm s}^2 + \theta_{\rm b}^2)$, where $\theta_{\rm b}$ and $\theta_{\rm s}$ are the beam and the source size. Following Wang et al., a source size of 40″ was assumed. Then we ran the RADEX code using the measured Δv to fit $T'_{\rm mb}$ for each transition. Figure 7 shows the RADEX calculations for the HCN, displaying the expected H_2 density and N(HCN) pairs that correspond to a given $T'_{\rm mb}$ and 4–3/3–2 intensity ratio. The calculations were made for kinetic temperatures of 20, 50, and 100 K, as in previous studies (see Wang et al. 2009 and references therein). The results from the $J = 4–3$ and $J = 3–2$ lines are presented in Table 5. The results from the $J = 3–2$ and $J = 1–0$ lines are similar to those obtained by Wang et al. (2009), that is, a density of several 10^5 cm^{-3}, and N(HCN) of about 1×10^{13} cm^{-2}. Thus we conclude that the HCN column density ranges from 1.4×10^{12} to about 1×10^{13} cm^{-2}, and the density varies from some 10^5 to a few 10^7 cm^{-3}. Our results confirm that the HCN emission arises from a very high density region in N113. The density of this region ranges between the HCO^+ and HCN $J = 4–3$ critical densities, which explains the dependency of the HCO^+/HCN ratio on the rotational transitions discussed above.

Table 5. Radex results from the HCN 4–3 and 3–2 lines.

T_k (K)	$n_{\rm H_2}$ (cm^{-3})	N(HCN) (cm^{-2})	τ_{4-3}	τ_{3-2}
20	2.51×10^7	1.47×10^{12}	0.014	0.018
50	3.23×10^6	1.38×10^{12}	0.014	0.019
100	1.82×10^6	1.43×10^{12}	0.014	0.020

4. Summary

The HII region N113 is located in the central part of the Large Magellanic Cloud (LMC) with an associated molecular cloud that is very rich in molecular species. Most of the molecular lines observed to date cover the frequency range 85–270 GHz, which means that a survey at higher frequencies in the 345 GHz window is required for a more complete understanding of the chemistry and excitation conditions of the region. To do this, we mapped a region of 2.′5×2.′5 centred on N113 using the Atacama Submillimeter Telescope Experiment in the ^{13}CO $J = 3–2$ line with an angular and spectral resolution of 22″ and 0.11 km s^{-1}, and observed 16 molecular lines as single pointings towards its centre. The main results are summarized as follows:

(1) The molecular cloud associated with N113 mapped in the ^{13}CO $J = 3–2$ line shows a curved and elongated morphology that agrees well with the IR emission. From this line we estimated LTE and virial masses for the molecular cloud of about 1×10^4 and 4.5×10^4 $M_\odot$, respectively. Additionally, from the dust continuum emission at 500 μm we obtained a gas mass of about 7×10^3 $M_\odot$.

(2) Towards the centre of the N113 molecular cloud we detected emission from ^{12}CO, ^{13}CO, C^{18}O (3–2), HCN, HNC, HCO^+, C_2H (4–3), and CS (7–6); this is the first reported detection of HCN, HNC, and C_2H in the $J = 4–3$ line from this region. We confirmed the detection of CS (7–6), which was previously tentatively detected. The detection of HCN (4–3) and CS (7–6) reveals a very high density region.

(3) The observed C_2H (4–3) presents two peaks due to its fine-structure transitions. We suggest that the chemistry involving C_2H in N113 is similar to the chemistry in Galactic PDRs.

(4) We found that the HCN/HNC ratio is higher than unity in the $J = 4–3$ line, as is the case for lower transitions, supporting the prediction that this ratio would be high in warm gas that is subject to strong UV heating, which in turn indicates a PDR scenario, which agrees with our finding of broad C_2H lines. Additionally, we found that HCO^+/HCN ratio increases with increasing rotational transitions, showing different critical densities for the two molecular species.

(5) Using the parameters derived from our HCN $J = 4–3$ observation and previous results from HCN $J = 3–2$ and $J = 1–0$, we performed a non-LTE study of this molecule. Our results confirm that the HCN emission arises from a very high density region in N113, with densities ranging between some 10^5 and 10^7 cm^{-3}.

Acknowledgements. We thank the anonymous referee for her/his helpful comments and corrections. The ASTE project is led by Nobeyama Radio Observatory (NRO), a branch of National Astronomical Observatory of Japan (NAOJ), in collaboration with University of Chile, and Japanese institutes including University of Tokyo, Nagoya University, Osaka Prefecture University, Ibaraki University, Hokkaido University, and the Joetsu University of Education. S.P. and M.O. are members of the *Carrera del investigador científico* of CONICET, Argentina. This work was partially supported by grants awarded by CONICET, ANPCYT and UBA (UBACyT) from Argentina. M.R. wishes to acknowledge support from CONICYT through FONDECYT grant No. 1140839.

References

Bekki, K., & Tsujimoto, T. 2010, ApJ, 721, 1515
Beuther, H., Semenov, D., Henning, T., & Linz, H. 2008, ApJ, 675, L33
Bica, E., Claria, J. J., & Dottori, H. 1992, AJ, 103, 1859
Book, L. G., Chu, Y.-H., Gruendl, R. A., & Fukui, Y. 2009, AJ, 137, 3599
Brooks, K. J., & Whiteoak, J. B. 1997, MNRAS, 291, 395
Carlson, L. R., Sewiło, M., Meixner, M., Romita, K. A., & Lawton, B. 2012, A&A, 542, A66
Chen, C.-H. R., Indebetouw, R., Chu, Y.-H., et al. 2010, ApJ, 721, 1206
Chin, Y.-N., Henkel, C., Whiteoak, J. B., et al. 1997, A&A, 317, 548
Ezawa, H., Kawabe, R., Kohno, K., & Yamamoto, S. 2004, SPIE Conf. Ser., 5489, ed. J. M. Oschmann, Jr., 763
Garay, G., Johansson, L., Nyman, L.-Å., et al. 2002, A&A, 389, 977
Gruendl, R. A., & Chu, Y.-H. 2009, ApJS, 184, 172
Heikkilä, A., Johansson, L., & Olofsson, H. 1999, A&A, 344, 817
Herrera, C. N., Rubio, M., Bolatto, A. D., et al. 2013, A&A, 554, A91
Hunter, I., Dufton, P. L., Smartt, S. J., et al. 2007, A&A, 466, 277
Imai, H., Katayama, Y., Ellingsen, S. P., & Hagiwara, Y. 2013, MNRAS, 432, L16
Johansson, L. E. B., Olofsson, H., Hjalmarson, A., Gredel, R., & Black, J. H. 1994, A&A, 291, 89
Jørgensen, J. K., Hogerheijde, M. R., Blake, G. A., et al. 2004, A&A, 415, 1021
Kastner, J. H., Buchanan, C., Sahai, R., Forrest, W. J., & Sargent, B. A. 2010, AJ, 139, 1993
Lazendic, J. S., Whiteoak, J. B., Klamer, I., Harbison, P. D., & Kuiper, T. B. H. 2002, MNRAS, 331, 969
MacLaren, I., Richardson, K. M., & Wolfendale, A. W. 1988, ApJ, 333, 821
Massey, P., Lang, C. C., Degioia-Eastwood, K., & Garmany, C. D. 1995, ApJ, 438, 188
Meixner, M., Gordon, K. D., Indebetouw, R., et al. 2006, AJ, 132, 2268
Meixner, M., Galliano, F., Hony, S., et al. 2010, A&A, 518, L71
Meixner, M., Panuzzo, P., Roman-Duval, J., et al. 2013, AJ, 146, 62
Miettinen, O. 2014, A&A, 562, A3
Papadopoulos, P. P. 2007, ApJ, 656, 792
Povich, M. S., Churchwell, E., Bieging, J. H., et al. 2009, ApJ, 696, 1278
Scoville, N. Z., Sargent, A. I., Sanders, D. B., et al. 1986, ApJ, 303, 416
Seale, J. P., Looney, L. W., Chu, Y.-H., et al. 2009, ApJ, 699, 150
Seale, J. P., Looney, L. W., Wong, T., et al. 2012, ApJ, 751, 42
Seaquist, E. R., & Frayer, D. T. 2000, ApJ, 540, 765
Sewiło, M., Indebetouw, R., Carlson, L. R., et al. 2010, A&A, 518, L73
Stacey, G. J., Geis, N., Genzel, R., et al. 1991, ApJ, 373, 423
Takakuwa, S., Ohashi, N., Bourke, T. L., et al. 2007, ApJ, 662, 431
van der Tak, F. F. S., Black, J. H., Schöier, F. L., Jansen, D. J., & van Dishoeck, E. F. 2007, A&A, 468, 627
Verdugo, C., Rubio, M., & Bolatto, A. 2011, Boletin de la Asociacion Argentina de Astronomia, 54, 247
Wang, M., Chin, Y.-N., Henkel, C., Whiteoak, J. B., & Cunningham, M. 2009, ApJ, 690, 580
Weingartner, J. C., & Draine, B. T. 2001, ApJ, 548, 296
Whiteoak, J. B., & Gardner, F. F. 1986, MNRAS, 222, 513
Wilcots, E. M. 1994, AJ, 108, 1674
Wong, T., Whiteoak, J. B., Ott, J., Chin, Y.-N., & Cunningham, M. R. 2006, ApJ, 649, 224